

## Highly Porous and Thermally Stable Poly(vinylidene fluoride) Separators : Effects of Solvent and Colloidal SiO<sub>2</sub> Concentration

Widiyandari, Hendri

Department of Physics, Faculty of Mathematics and Natural Sciences, Sebelas Maret University

Okie Ade Putra

Department of Physics, Faculty of Mathematics and Natural Sciences, Sebelas Maret University

Suryana, Risa

Department of Physics, Faculty of Mathematics and Natural Sciences, Sebelas Maret University

Firdaus, Iqbal

Department of Physics, Faculty of Mathematics and Natural Sciences, Lampung University

<https://doi.org/10.5109/4794170>

---

出版情報 : Evergreen. 9 (2), pp.443-450, 2022-06. 九州大学グリーンテクノロジー研究教育センター  
バージョン :

権利関係 : Creative Commons Attribution-NonCommercial 4.0 International



# Highly Porous and Thermally Stable Poly(vinylidene fluoride) Separators : Effects of Solvent and Colloidal SiO<sub>2</sub> Concentration

Hendri Widiyandari<sup>1, 2,\*</sup>, Oki Ade Putra<sup>1</sup>, Risa Suryana<sup>1</sup>, Iqbal Firdaus<sup>3</sup>

<sup>1</sup>Department of Physics, Faculty of Mathematics and Natural Sciences, Sebelas Maret University, Indonesia

<sup>2</sup>Centre of Excellence for Electrical Energy Storage Technology, Sebelas Maret University, Indonesia

<sup>3</sup>Department of Physics, Faculty of Mathematics and Natural Sciences, Lampung University, Indonesia

\*Author to whom correspondence should be addressed:

Email: hendriwidiyandari@staff.uns.ac.id

(Received December 7, 2021; Revised June 3, 2022; accepted June 3, 2022).

**Abstract:** Separator is an important part of lithium-ion batteries because it acts both as a physical barrier for the electrodes and as an electrolyte reservoir for ion transport. The separator has direct influence on the battery performance. Polyolefins, typical materials used for the fabrication of separator, demonstrate high flexibilities and mechanical strengths but also possess a high ratio of thermal shrinkage and low porosity. The aim of the research is to obtain highly porous and thermally stable separator. Poly(vinylidene fluoride) (PVDF) nanofiber membrane was synthesized via double jet electrospinning method. PVDF was dissolved in variations of solvents, i.e., dimethylformamide-acetone and dimethylformamide-ethanol and added with colloidal SiO<sub>2</sub> at different concentrations of 0 ppm, 1000 ppm, 3000 ppm, and 5000 ppm. The obtained separators exhibited high porosities, high electrolyte uptakes, and thermally stable, resulting in improved performances when assembled in real battery cell systems.

**Keywords:** Electrospinning, separator, poly(vinylidene fluoride)/SiO<sub>2</sub>, nanofiber, lithium-ion battery

## 1. Introduction

The global demand for rechargeable batteries is expected to reach nearly 1000 GWh per year by 2025 <sup>1)</sup>. Among the battery cells, lithium-ion batteries are not only applied in mobile devices such as camera and mobile phones <sup>2)</sup> but also in complex operating systems, including electric vehicles <sup>3)</sup> and energy storage in renewable energy power plants. They offer some distinct advantages, including long lifetimes <sup>4)</sup>, low self-discharges, high energy densities <sup>5)</sup>, high efficiencies <sup>6)</sup>, and good cycle performances <sup>7)</sup>, which are responsible for the diverse applications.

The lithium-ion battery has four main components: the positive electrode (cathode) is a lithium-based metal-oxide; the negative electrode (anode) consists of an active material collecting the ions; the liquid electrolyte enables the lithium-ion transfer between cathode and anode; finally, a separator assures battery safety by preventing the contact between the two electrodes.

Although it does not have to be an electrochemically active component within the cell, the separator plays an important role in lithium-ion transport, affecting rate performance, cell life, and safety. First, a suitable

separator must be characterized by a high ionic conductivity <sup>8)</sup>. Furthermore, to improve the battery safety, solid electrolytes can be employed <sup>9)</sup>. However, there are limitations that are hindering the large-scale production of these systems, such as low ionic conductivities, poor interface contacts, and the absence of effective ways of mass production <sup>10)</sup>. To overcome these drawbacks, a separator characterized by adequate thermal stability was used.

Currently, commercial separators mostly employ poly(ethylene) (PE) <sup>11)</sup>, poly(propylene) (PP) <sup>12)</sup>, and poly(ethylene oxide) (PEO) <sup>13)</sup>, owing to their affordable prices and excellent mechanical properties. However, insufficient porosities and poor resistances to high temperatures are the main drawbacks of these polyolefins. Due to their low melting points (408.15 K, 438.15 K, and 338.15 K for PE, PP, and PEO, respectively <sup>14)</sup>), when the battery is used under high-temperature conditions, the pores of the polymeric separator are rapidly blocked. This condition is dangerous because it causes the disruption of the electrochemical processes and internal short circuits, which are potential causes of fire.

In this research, we processed poly(vinylidene fluoride) (PVDF), characterized by a high melting point (450.15 K),

into nanofiber membranes. These materials have been synthesized via several routes, including melt-blow<sup>15)</sup>, wet-laid<sup>16)</sup>, vacuum filtration<sup>17)</sup>, and electrospinning<sup>18)</sup>. Particularly, electrospinning is a straightforward manufacturing technique to prepare nanofibers via an electrostatically driven process. We optimized the process by tuning the PVDF solvent and colloidal SiO<sub>2</sub> concentration. The solvent choice was based on previous studies showing that PVDF dissolved in dimethylformamide (DMF) resulted in larger fiber diameters<sup>19)</sup> compared to PVDF dissolved in DMF/acetone<sup>20)</sup>. However, the high acetone vapor pressure allows for the variations of PVDF polymer concentrations; therefore, DMF-ethanol solvent was used as a comparison. The addition of colloidal SiO<sub>2</sub> enables the membrane porosity and wettability enhancement<sup>21)</sup>. Furthermore, addition of colloidal SiO<sub>2</sub> can improve the quality of the nanofiber membrane as a battery separator, such as the resistance of the nanofiber membrane to high temperatures<sup>22)</sup>.

## 2. Materials and Methods

### 2.1 Materials

The following materials were used: poly(vinylidene fluoride) (C<sub>2</sub>H<sub>2</sub>F<sub>2</sub>)<sub>n</sub>, (PA, Aldrich), *N,N*-dimethylformamide (PA, Merck), acetone (PA, Merck), ethanol (PA, Merck), tetraethylorthosilicate (TEOS) (PA, Merck 99 %), distilled water, acetic acid (PA, Merck), and microporous Celgard-2400 separator (PP, Celgard).

### 2.2 Methodology

#### 2.2.1 Preparation of PVDF solutions

Table 1. The samples preparation condition.

Sample Code	PVDF Solvent	SiO <sub>2</sub> Concentration [ppm]
PVDF-A	DMF/acetone	0
PVDF-A/SiO <sub>2</sub> 1000	DMF/acetone	1000
PVDF-A/SiO <sub>2</sub> 3000	DMF/acetone	3000
PVDF-A/SiO <sub>2</sub> 5000	DMF/acetone	5000
PVDF-E	DMF/ethanol	0
PVDF-E/SiO <sub>2</sub> 1000	DMF/ethanol	1000
PVDF-E/SiO <sub>2</sub> 3000	DMF/ethanol	3000
PVDF-E/SiO <sub>2</sub> 5000	DMF/ethanol	5000
PP	Microporous Celgard 2400 separator	

The nanofiber membrane preparation comprised three steps, as depicted in Fig. 1: the synthesis of PVDF polymer solution and colloidal SiO<sub>2</sub>, double jet electrospinning process, and membrane drying process. The synthesis was performed by dissolving PVDF (15 wt.%) in DMF-acetone (named PVDF-A) or DMF-ethanol (named PVDF-E) at a volume ratio of 7:3. Afterwards, the precursor solution was stirred at 333.15 K for 8 h, until a homogeneous solution was obtained. The samples prepared with various solvents and SiO<sub>2</sub>

concentrations are shown in Table 1.

#### 2.2.2 Synthesis of colloidal SiO<sub>2</sub> and electrospinning process

Colloidal SiO<sub>2</sub> was prepared following a sol-gel method<sup>23)</sup>. TEOS (18 ml), acetic acid (36 ml) and distilled water (6.4 ml) were mixed together; the obtained solution was aged until the formation of a colloidal gel. This was subsequently washed with ethanol and filtered, leading to the formation of a SiO<sub>2</sub> residue. Afterwards, SiO<sub>2</sub> was dissolved in DMF with varying concentrations of 0, 1000, 3000, and 5000 ppm. Nanofiber membranes were synthesized using a double jet electrospinning method for 2 h on a rotating cylinder collector, with the following electrospinning parameters: a high voltage of 15 kV, a collector rotational speed of 150 rpm, and a tip-to-collector distance of 17 cm. These parameters are used in both electrospinning processes, the only difference being the PVDF flow rate is 1.5 ml/h while the SiO<sub>2</sub> flow rate is 0.5 ml/h. The resulting PVDF/SiO<sub>2</sub> nanofiber membranes were then dried for 24 h.

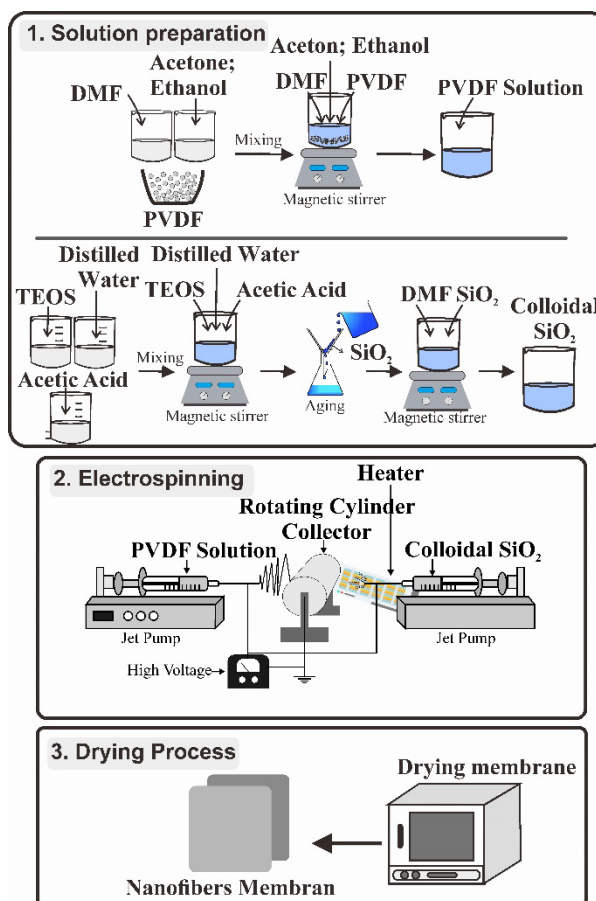


Fig. 1: Experimental method for synthesis of PVDF/SiO<sub>2</sub> nanofiber membrane.

#### 2.2.3 Sample characterization

The functional groups of the starting materials and samples were analyzed via Fourier-transform infrared

(FTIR) spectroscopy using a Shimadzu IRSpirit Spectrophotometer, Japan. The morphology of the samples was characterized with a JEOL Benchtop JCM-7000 scanning electron microscopy (SEM), Japan. Measurement of fiber diameter using Image-J software by measuring 100 fiber separators. The membrane was cut into 2 x 2 cm squares and then immersed in a solution of *n*-butanol for 2 hours to test porosity. The membrane porosity was calculated using Equation 1<sup>24)</sup>

$$P = \frac{W_{wet} - W_{dry}}{\rho V} \times 100\% \quad (1)$$

where  $W_{wet}$  is the weight of the wet membrane after immersion,  $W_{dry}$  is the weight of the dry membrane,  $\rho$  is the density of *n*-butanol, and  $V$  is the membrane volume.

The membrane electrolyte uptake was tested by immersing the samples in a LiPF<sub>6</sub> electrolyte in the glove box for 2 hours. The electrolyte uptake was calculated using Equation 2<sup>25)</sup>.

$$SE = \frac{W_f - W_i}{W_i} \times 100\% \quad (2)$$

where  $W_i$  and  $W_f$  are the membrane weights before and after immersion in the electrolyte, respectively.

The membrane shrinkage ratio was tested using a 2.7 cm diameter circle membrane heated at 423.15 K for 30 min. The membrane shrinkage was calculated using Equation 3<sup>26)</sup>.

$$S = \frac{A_b - A_a}{A_b} \times 100\% \quad (3)$$

where  $S$  is the membrane shrinkage area, and  $A_b$  and  $A_a$  are the membrane area before and after heating, respectively.

The evaluated mechanical properties of the samples were the tensile strength and elongation of the membrane. The mechanical properties test used a standard form with ASTM code D638-02A by using the Autograph AG-10TE test tool. The battery performance was tested using a cylinder cell with nickel manganese cobalt (NMC) as cathode, graphite as anode, and LiPF<sub>6</sub> as electrolyte. The charge-discharge and cycle test were performed using battery analyzer (Neware, China).

### 3. Results and Discussion

FTIR analysis are used to identify bonding vibration of the functional groups present in the nanofiber membrane. The spectra of all samples are characterized by three intense peaks at 1280–1110 cm<sup>-1</sup>, 1461–1346 cm<sup>-1</sup>, and 878 cm<sup>-1</sup> (Fig. 2 and Fig. 3). The former two peaks refer to the typical CF<sub>2</sub> and CH<sub>2</sub> modes in PVDF<sup>27,28)</sup>. Moreover,

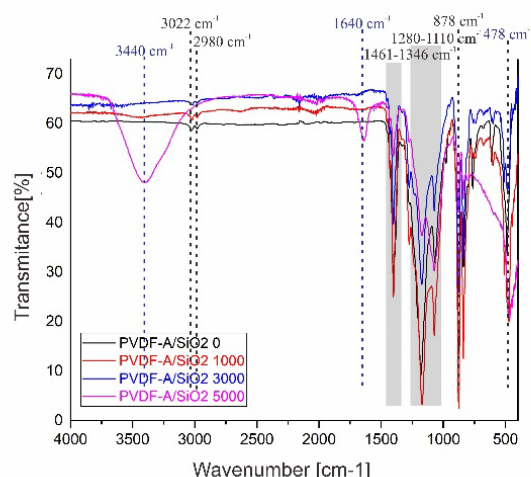


Fig. 2: FTIR spectra of PVDF-A/SiO<sub>2</sub>

the first peak overlaps with SiO<sub>2</sub> modes<sup>29)</sup>, while the latter peaks at 878 cm<sup>-1</sup> overlaps with the C–F strain vibration mode of PVDF<sup>30)</sup> and the characteristic peak of Si–O–Si of SiO<sub>2</sub><sup>31)</sup>. The additional weak peaks at 3022 cm<sup>-1</sup> and 2980 cm<sup>-1</sup> were assigned to the CH<sub>2</sub> asymmetric and symmetric vibration modes of PVDF<sup>30)</sup>, respectively.

The addition of colloidal SiO<sub>2</sub> to the PVDF-A/SiO<sub>2</sub> and PVDF-E/SiO<sub>2</sub> membranes led to the appearance of the broad peaks at 3440–3420 cm<sup>-1</sup> and 1640–1630 cm<sup>-1</sup> assigned to the –OH modes of SiO<sub>2</sub><sup>32)</sup>. These peaks indicate the bonding between SiO<sub>2</sub> oxygen atoms and PVDF hydrogen atoms, occurring during electrospinning. FTIR analysis performed in the range of 400–4000 cm<sup>-1</sup> confirmed the successful preparation of the membranes, bearing the typical functional groups of PVDF and SiO<sub>2</sub>.

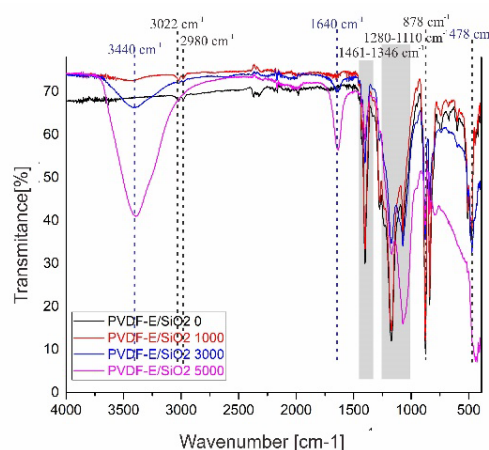
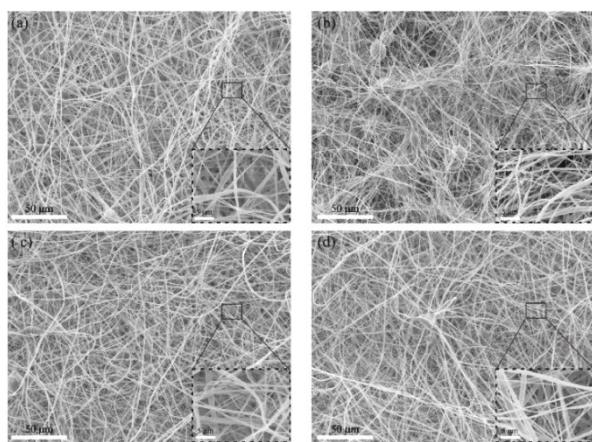


Fig. 3: FTIR spectra of PVDF-E/SiO<sub>2</sub>

Fig. 4 and Fig. 5 show the SEM images with 500 times magnification for PVDF-A/SiO<sub>2</sub> and PVDF-E/SiO<sub>2</sub> membranes, respectively. The electrospinning led to the formation of beads, as revealed by the closer inspection of the images (bottom right: enlarged areas). Notably, the



formation of beaded membranes negatively affects the uniformity of the nanofiber membrane <sup>33</sup>). For samples with SiO<sub>2</sub> 0 ppm (Fig. 4 (a) and Fig. 5 (a)), the formation of beads was limited by the high net charge density (NCD) factor <sup>34</sup>). Nevertheless, the high NCD values for the samples with SiO<sub>2</sub> 0 ppm were caused by the electrospinning using a single jet, so that the applied voltage was not divided, rather than by the addition of colloidal SiO<sub>2</sub>. Increasing SiO<sub>2</sub> concentration (Fig. 4(b-d) and Fig. 5(b-d)) did not affect bead formation because for these samples, a double-jet pump was employed in the electrospinning process. For all samples, the small SiO<sub>2</sub> particle size allowed the colloid to stick to the fiber surface.



**Fig. 4:** Morphology of PVDF-A/SiO<sub>2</sub> a) 0 ppm; b) 1000 ppm; c) 3000 ppm; d) 5000 ppm. Inset shows the higher magnification of each sample.

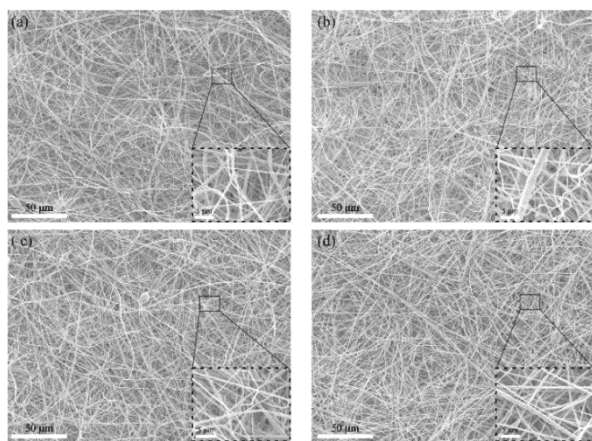


**Fig. 5:** Morphology of PVDF-E/SiO<sub>2</sub> a) 0 ppm; b) 1000 ppm; c) 3000 ppm; d) 5000 ppm. Inset shows the higher magnification of each sample.

The fiber diameter was obtained by measuring the fiber size from the SEM images using ImageJ software. Fig. 6 shows the fiber size distribution of PVDF-A/SiO<sub>2</sub> and PVDF-E/SiO<sub>2</sub>. The PVDF-A/SiO<sub>2</sub> (Fig. 6 (a)) fiber size was smaller than that obtained for PVDF-E/SiO<sub>2</sub> membranes (Fig. 6 (b)). Since the fiber diameter size is

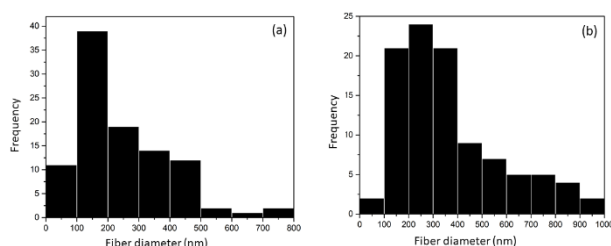


**Fig. 6:** Fiber size distribution of a) PVDF-A/SiO<sub>2</sub> and b) PVDF-E/SiO<sub>2</sub>.

directly correlated to the solution viscosity <sup>35</sup>), the viscosity difference between acetone and ethanol affected the measured fiber size. Specifically, at 295.15 K, the viscosity of acetone (0.3 mPa·s) <sup>36</sup> is lower than that of ethanol (1.1 mPa·s) <sup>37</sup>. The average diameters for PVDF-A/SiO<sub>2</sub> and PVDF-E/SiO<sub>2</sub> membranes were ~254.14 nm and ~336.54 nm, respectively.

Porosity, electrolyte uptake, and fiber size uniformity are important parameters affecting the specific capacity of a battery <sup>38</sup>). For all membranes, the obtained porosities and electrolyte uptakes reported in Table 2 were higher than the corresponding values obtained for the commercial separator selected as a comparison (PP, 38 ± 6 %). Nanofiber membranes have smaller fiber sizes and higher porosities than non-woven membranes, such as PP <sup>24</sup>).

For both nanofiber membrane types, the addition of SiO<sub>2</sub> increased the porosities and electrolyte uptakes. The porosity increase is ascribable to two main factors: first, SiO<sub>2</sub> porous structure (pore diameter ~7 nm <sup>39</sup>) acts as a lithium-ion reservoir. Second, the position of SiO<sub>2</sub> on the fiber surface reduces the distance between the fibers (pores). Therefore, the porosity and the electrolyte uptake of the material increase.

Table 2. Porosities and electrolyte uptakes for the prepared nanofiber membranes and the commercial PP separator.

Membrane s Separator	Porosity [%]		Electrolyte Uptake [%]	
	PVDF-A	PVDF-E	PVDF-A	PVDF-E
SiO <sub>2</sub> 0	60 ± 1.6	54 ± 1.5	779 ± 10	787 ± 12
SiO <sub>2</sub> 1000	73 ± 2.1	56 ± 1.9	961 ± 14	683 ± 14
SiO <sub>2</sub> 3000	79 ± 2.4	64 ± 2.5	1198 ± 28	843 ± 24
SiO <sub>2</sub> 5000	82 ± 2.2	71 ± 2.8	1265 ± 31	1181 ± 28
PP	38 ± 3.4		184 ± 12	

Noticeably, the porosity and electrolyte uptake of PVDF-A/SiO<sub>2</sub> are higher than those of PVDF-E/SiO<sub>2</sub>, which is agreement with the difference in fiber sizes. Previous studies <sup>40</sup>) correlated the small fiber size to a limited pore size. Accordingly, a reduction in the pore size caused the membrane porosity to increase and a consequent enhancement in the electrolyte uptake <sup>33</sup>). Significantly, the porosities and electrolyte uptakes of PVDF/SiO<sub>2</sub> membranes were higher than those of other

membrane composites, such as PVDF/polyimide and PVDF/triphenyl phosphate-cellulose acetate<sup>41)</sup>.

The results of the membrane-shrinkage-ratio tests are shown in Table 3, while Fig. 7 shows the nanofiber membranes before and after heating.

Table 3. Shrinkage ratio of nanofiber membranes and PP separator.

Membran separator	Shrinkage ratio [%]	
	PVDF-A	PVDF-E
SiO <sub>2</sub> 0	21.8 ± 1.8	9.1 ± 1.9
SiO <sub>2</sub> 1000	11.9 ± 2.1	1.4 ± 2.1
SiO <sub>2</sub> 3000	1.9 ± 2.3	0
SiO <sub>2</sub> 5000	0	0
PP	Damaged sample	

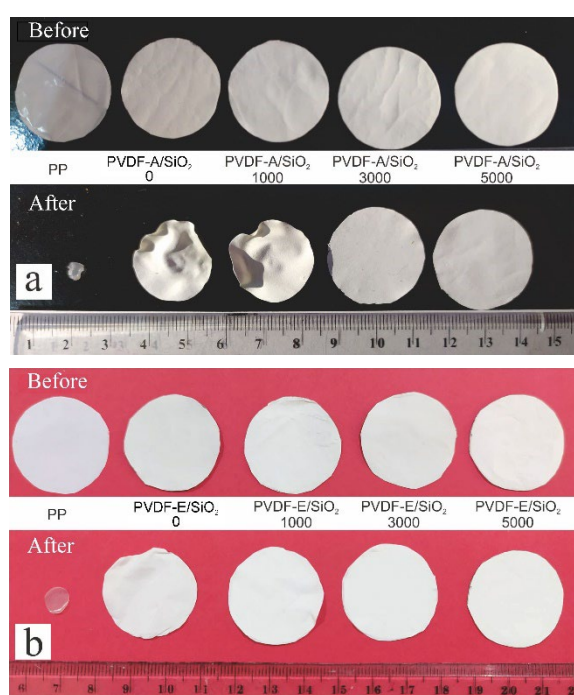


Fig. 7. Shrinkage effects on membrane dimensions for a) PVDF-A/SiO<sub>2</sub> and b) PVDF-E/SiO<sub>2</sub> before and after heating at 423.15 K. Comparison with the commercially available PP separator is provided.

Compared to the PVDF/SiO<sub>2</sub> membranes, PP separators could not withstand the operating temperature condition of 423.15 K, and its shrinkage was completed within ~8 min. The main factors favoring the PVDF/SiO<sub>2</sub> membranes over the PP separator at high temperatures are the high melting point (450.15 K), high heat transition (approximately 393.15–433.15 K<sup>42)</sup>), and thermal stability of PVDF<sup>43)</sup>.

As shown in Fig. 7 (a) and (b), the increase in the colloidal SiO<sub>2</sub> concentration led to an enhancement in the ability of the membrane to retain its original dimension. The high melting point of SiO<sub>2</sub> (1983.15 K) influenced the membrane shrinkage. Moreover, the thermal stability was highly affected by the boiling point of the solvent. Acetone has a lower boiling point (329.15 K) and a higher

vapor pressure (30.6 kPa<sup>44)</sup>), compared to ethanol (351.15 K and 5.95 kPa<sup>45)</sup>, respectively). Consequently, ethanol persistency in the membrane contributes to the enhancement of the membrane thermal stability. The low thermal conductivity, determined by the pore size, porosity distributions and for the membrane shrinkage. The small pore size and high porosity of the membrane are related to a low thermal conductivity<sup>46)</sup>. Therefore, the high thermal stabilities of PVDF-E/SiO<sub>2</sub> membranes were explained by considering all these factors.

Furthermore, the tensile strength was measured for the prepared samples and the PP separator, and the results of this research are listed in Table 4. Notably, PP separator was characterized by a higher tensile strength, compared to all the PVDF/SiO<sub>2</sub> nanofiber membranes. The increasing concentration of the SiO<sub>2</sub> sol affects the tensile strength of the membrane. Moreover, the addition of SiO<sub>2</sub> improved the tensile strength and other mechanical properties of the prepared membranes, as previously reported<sup>47,48)</sup>. The increasing tensile strength of the membrane is due to SiO<sub>2</sub> inserting into the pores and causing the pore size to decrease, increasing the membrane's tightness and strength.

Table 4. Mechanical properties of nanofiber membranes.

Membrane separator	Tensile strength [MPa]		Elongation [%]	
	PVDF-A	PVDF-E	PVDF-A	PVDF-E
SiO <sub>2</sub> 0	0.83	0.006	11	35
SiO <sub>2</sub> 1000	1.19	0.019	10	46
SiO <sub>2</sub> 3000	1.53	0.01	7	31
SiO <sub>2</sub> 5000	2.20	0.02	12	38
PP	41.30		16	

Table 4 shows the improved tensile strengths of PVDF-A membranes, compared to those of PVDF-E membranes. This is ascribable to the higher moisture content of the PVDF-E membranes negatively affecting their tensile strengths.

Concerning the elongation tests, the results reported in Table 4 show a negligible effect of the addition of SiO<sub>2</sub> on the membrane elongation for all the prepared samples. Among the acetone membranes, the highest elongation rate was reached by PVDF/SiO<sub>2</sub> 5000 ppm (12 %), while among the ethanol membranes, the highest elongation rate was exhibited by PVDF/SiO<sub>2</sub> 1000 ppm (46 %). However, both PVDF-A/SiO<sub>2</sub> and PVDF-E/SiO<sub>2</sub> nanofiber membranes had relatively unchanged percentage elongation values before and after the addition of colloidal SiO<sub>2</sub>. This situation proves that the addition of colloidal SiO<sub>2</sub> concentration does not reduce the membrane elongation ability so that it can provide advantages during the lithium-ion battery assembly process. During the assembly of a cylindrical battery, the membrane and electrodes will be pulled and rolled so that the ability of mechanical properties has an important contribution in battery assembly.

Battery performance testing was carried out on the samples with the best properties for each solvent, namely PVDF-A/SiO<sub>2</sub> 5000 ppm and PVDF-E/SiO<sub>2</sub>, and microporous Celgard separator 2400 was used as a comparison. The graph of the charge-discharge test is shown in Fig. 8.

Lithium-ion battery using a PVDF-E/SiO<sub>2</sub> membrane separator exhibited the smallest specific capacity (1.76 mAh/g), among all the samples tested. Concurrently, PVDF-A/SiO<sub>2</sub> membrane and PP separator showed high specific capacities (195.3 mAh/g and 195.0 mAh/g, respectively). The lowest specific capacity of PVDF-E/SiO<sub>2</sub> was due to membrane damage during the battery assembly. To compare the battery performance stabilities, the retention ratios were calculated based on the graph in Fig. 9.

The battery stability was measured to determine the specific capacity of each cycle. A smaller specific capacity decrease of the battery was related to a higher retention ratio. This parameter was obtained by comparing the capacity of the last and first cycles. The measured

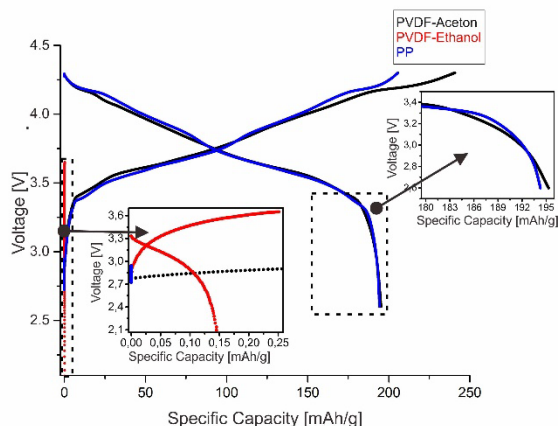


Fig. 8. Lithium-ion battery charge-discharge test.

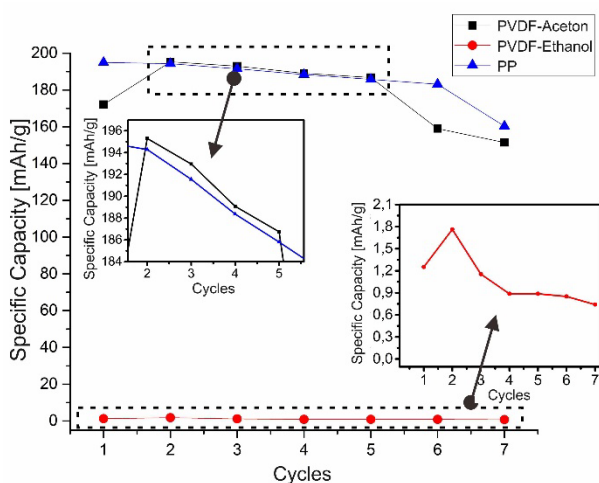


Fig. 9. Retention ratio of lithium-ion battery.

retention ratios were 88 %, 59 %, and 82 % for PVDF-A/SiO<sub>2</sub>, PVDF-E/SiO<sub>2</sub> and PP, respectively. The high

retention ratio of PVDF-A/SiO<sub>2</sub> indicates its stable specific capacity. The low retention ratio measured for PVDF-E/SiO<sub>2</sub> is due to the obstruction of the lithium-ion transport between the electrodes in this separator.

## 4. Conclusions

PVDF/SiO<sub>2</sub> nanofiber membranes were successfully synthesized via the double-jet electrospinning method. Owing to the small fiber diameter, PVDF-A/SiO<sub>2</sub> membranes exhibited higher porosities, electrolyte uptakes, and tensile strengths than PVDF-E/SiO<sub>2</sub> samples. However, in the shrinkage ratio analyses at high temperatures, PVDF-E performed better because of its higher thermal conductivity than the other samples. Overall, PVDF-A/SiO<sub>2</sub> nanofiber membrane showed the best battery performance, compared to the commercial PP separator and the PVDF-E/SiO<sub>2</sub> nanofiber membranes.

## Acknowledgements

This research was funded by the Ministry of Education, Culture, Research, and Technology, Republic of Indonesia, Penelitian Dasar Unggulan Perguruan Tinggi (PDUPT), contract numbers 11/E1/KP.PTNBH/2021 and 221.1/UN27.22/HK.07.00/2021.

## References

- 1) M. Abdelbaky, J.R. Peeters, and W. Dewulf, "On the influence of second use, future battery technologies, and battery lifetime on the maximum recycled content of future electric vehicle batteries in europe," *Waste Manag.*, **125**, 1–9 (2021). doi:10.1016/j.wasman.2021.02.032.
- 2) M. Torabi, S.H. Razavi, and S. Sanjabi, "Electrochemical evaluation of pbo nanoparticles as anode for lithium ion batteries," *Int. J. Eng. Trans. B Appl.*, **24** (4) 351–355 (2011). doi:10.5829/idosi.ije.2011.24.04b.05.
- 3) P. Zhu, D. Gastol, J. Marshall, R. Sommerville, V. Goodship, and E. Kendrick, "A review of current collectors for lithium-ion batteries," *J. Power Sources*, **485** (November 2020) 229321 (2021). doi:10.1016/j.jpowsour.2020.229321.
- 4) L. Wang, Q. Wang, W. Jia, S. Chen, P. Gao, and J. Li, "Li metal coated with amorphous li<sub>3</sub>po<sub>4</sub> via magnetron sputtering for stable and long-cycle life lithium metal batteries," *J. Power Sources*, **342** 175–182 (2017). doi:10.1016/j.jpowsour.2016.11.097.
- 5) Z. Huang, C. Zhao, H. Li, W. Peng, Z. Zhang, and Q. Wang, "Experimental study on thermal runaway and its propagation in the large format lithium ion battery module with two electrical connection modes," *Energy*, **205** 117906 (2020). doi:10.1016/j.energy.2020.117906.
- 6) Y. Tian, L. Xu, J. Bao, J. Qian, H. Su, H. Li, H. Gu, C. Yan, and H. Li, "Hollow cobalt oxide nanoparticles



- embedded in nitrogen-doped carbon nanosheets as an efficient bifunctional catalyst for zn-air battery," *J. Energy Chem.*, **33** 59–66 (2019). doi:10.1016/j.jechem.2018.08.007.
- 7) G. Zhang, X. Wei, G. Han, H. Dai, J. Zhu, X. Wang, X. Tang, and J. Ye, "Lithium plating on the anode for lithium-ion batteries during long-term low temperature cycling," *J. Power Sources*, **484** 229312 (2021). doi:10.1016/j.jpowsour.2020.229312.
  - 8) P. Zhai, K. Liu, Z. Wang, L. Shi, and S. Yuan, "Multifunctional separators for high-performance lithium ion batteries," *J. Power Sources*, **499** (May) 229973 (2021). doi:10.1016/j.jpowsour.2021.229973.
  - 9) W. Zhao, J. Yi, P. He, and H. Zhou, "Solid - state electrolytes for lithium - ion batteries : fundamentals , challenges and perspectives," *Electrochem. Energy Rev.*, **2** (4) 574–605 (2019). doi:10.1007/s41918-019-00048-0.
  - 10) K. Takada, "Progress in solid electrolytes toward realizing solid-state lithium batteries," *J. Power Sources*, **394** 74–85 (2018). doi:10.1016/j.jpowsour.2018.05.003.
  - 11) J.M. Ko, E.G. Min, D.W. Kim, K.S. Ryu, K.M. Kim, Y.G. Lee, and S.H. Chang, "Thin-film type li-ion battery, using a polyethylene separator grafted with glycidyl methacrylate," *Electrochim. Acta*, **50** 367–370 (2004). doi:10.1016/j.electacta.2004.01.127.
  - 12) S. Yang, J. Gu, and Y. Yin, "A biaxial stretched  $\beta$ -isotactic polypropylene microporous membrane for lithium-ion batteries," *J. Appl. Polym. Sci.*, **135** (6) 45825 (2018). doi:10.1002/app.45825.
  - 13) C.H. Tsao, Y.H. Hsiao, C.H. Hsu, and P.L. Kuo, "Stable lithium deposition generated from ceramic-cross-linked gel polymer electrolytes for lithium anode," *ACS Appl. Mater. Interfaces*, **8** (24) 15216–15224 (2016). doi:10.1021/acsami.6b02345.
  - 14) T. Zhang, X.B. Cheng, Q. Zhang, Y. Lu, and G. Luo, "Construction of a cathode using amorphous fepo<sub>4</sub> nanoparticles for a high-power/energy-density lithium-ion battery with long-term stability," *J. Power Sources*, **324** 52–60 (2016). doi:10.1016/j.jpowsour.2016.05.071.
  - 15) H. Zhang, Q. Zhen, Y. Liu, R. Liu, and Y. Zhang, "Results in physics one-step melt blowing process for pp / peg micro-nano fi ber fi lters with branch networks," **12** (November 2018) 1421–1428 (2019). doi:10.1016/j.rinp.2019.01.012.
  - 16) F. Kessel, L. Klopsch, V. Jehle, N. Biller, M. Frie, Y. Shi, D. Cepli, M. Keck, and R. Jemmali, "Journal of the european ceramic society wet-laid nonwoven based ceramic matrix composites : an innovative and highly adaptable short fiber reinforcement for ceramic hybrid and gradient materials," *J. Eur. Ceram. Soc.*, **41** (February) 4048–4057 (2021). doi:10.1016/j.jeurceramsoc.2021.02.040.
  - 17) Z. Wang, R. Pan, C. Ruan, K. Edström, M. Strømme, and L. Nyholm, "Redox-active separators for lithium-ion batteries," *Adv. Sci.*, **1700663** (2017). doi:10.1002/advs.201700663.
  - 18) H. Widiyandari, O.A. Putra, A. Purwanto, and Z. Abidin, "Materials today : proceedings synthesis of pvdf/sio<sub>2</sub> nanofiber membrane using electrospinning method as a li-ion battery separator," *Mater. Today Proc.*, **44** 3245–3248 (2021). doi:10.1016/j.matpr.2020.11.448.
  - 19) Y. Yang, Y. Li, L. Cao, Y. Wang, L. Li, and W. Li, "Electrospun pvdf-sio<sub>2</sub> nanofibrous membranes with enhanced surface roughness for oil-water coalescence separation," *Sep. Purif. Technol.*, **269** 118726 (2021). doi:10.1016/j.seppur.2021.118726.
  - 20) H. Lee, M. Alcoutlabi, J. V. Watson, and X. Zhang, "Electrospun nanofiber-coated separator membranes for lithium-ion rechargeable batteries," *J. Appl. Polym. Sci.*, **129** (4) 1939–1951 (2013). doi:10.1002/app.38894.
  - 21) Y. Ma, J. Hu, Z. Wang, Y. Zhu, X. Ma, and C. Cao, "Poly(vinylidene fluoride)/SiO<sub>2</sub> composite membrane separators for high-performance lithium-ion batteries to provide battery capacity with improved separator properties," *J. Power Sources*, **451** 227759 (2020). doi:10.1016/j.jpowsour.2020.227759.
  - 22) M. Yanilmaz, Y. Lu, J. Zhu, and X. Zhang, "Silica/polyacrylonitrile hybrid nanofiber membrane separators via sol-gel and electrospinning techniques for lithium-ion batteries," *J. Power Sources*, **313** 205–212 (2016). doi:10.1016/j.jpowsour.2016.02.089.
  - 23) H.N. Azlina, J.N. Hasnidawani, H. Norita, and S.N. Surip, "Synthesis of sio<sub>2</sub> nanostructures using sol-gel method," *Acta Phys. Pol. A*, **129** (4) 842–844 (2016). doi:10.12693/APhysPolA.129.842.
  - 24) M. Yanilmaz, M. Dirican, and X. Zhang, "Evaluation of electrospun sio<sub>2</sub>/nylon 6,6 nanofiber membranes as a thermally-stable separator for lithium-ion batteries," *Electrochim. Acta*, **133** 501–508 (2014). doi:10.1016/j.electacta.2014.04.109.
  - 25) J. Lee, C. Lee, K. Park, and I. Kim, "Synthesis of an al 2 o 3 -coated polyimide nano fi ber mat and its electrochemical characteristics as a separator for lithium ion batteries," *J. Power Sources*, **248** 1211–1217 (2014). doi:10.1016/j.jpowsour.2013.10.056.
  - 26) C. Yang, H. Tong, C. Luo, S. Yuan, and G. Chen, "Boehmite particle coating modi fi ed microporous polyethylene membrane : a promising separator for lithium ion batteries," *J. Power Sources*, **348** 80–86 (2017). doi:10.1016/j.jpowsour.2017.02.078.
  - 27) X. Chen, B. Zhao, L. Zhao, S. Bi, P. Han, X. Feng, and L. Chen, "Temperature- and ph-responsive properties of poly(vinylidene fluoride) membranes functionalized by blending microgels," *RSC Adv.*, **4** (56) 29933–29945 (2014). doi:10.1039/c4ra02724h.
  - 28) Y. He, X. Chen, S. Bi, W. Fu, C. Shi, and L. Chen, "Conferring ph-sensitivity on poly (vinylidene fluoride) membrane by poly (acrylic acid-co-butyl



- acrylate) microgels,” *React. Funct. Polym.*, **74** (1) 58–66 (2014). doi:10.1016/j.reactfunctpolym.2013.10.012.
- 29) S.H. Tohidi, A.J. Novinrooz, and A. Nabipour, “Effect of inorganic hybrid lib on the silica matrix xerogels,” *Int. J. Eng. Trans. B Appl.*, **25** (1) 51–55 (2012). doi:10.5829/idosi.ije.2012.25.01b.06.
- 30) H. Bai, X. Wang, Y. Zhou, and L. Zhang, “Progress in natural science : materials international preparation and characterization of poly ( vinylidene fluoride ) composite membranes blended with nano-crystalline cellulose,” *Prog. Nat. Sci. Mater. Int.*, **22** (3) 250–257 (2012). doi:10.1016/j.pnsc.2012.04.011.
- 31) Y. Li, Q. Li, and Z. Tan, “A review of electrospun nanofiber-based separators for rechargeable lithium-ion batteries,” *J. Power Sources*, **443** 227262 (2019). doi:10.1016/j.jpowsour.2019.227262.
- 32) I. Ramalla, R.K. Gupta, and K. Bansal, “Effect on superhydrophobic surfaces on electrical porcelain insulator, improved technique at polluted areas for longer life and reliability,” *Int. J. Eng. Technol.*, **4** (4) 509–519 (2015). doi:10.14419/ijet.v4i4.5405.
- 33) X. Ma, P. Kolla, R. Yang, Z. Wang, Y. Zhao, A.L. Smirnova, and H. Fong, “Electrospun polyacrylonitrile nanofibrous membranes with varied fiber diameters and different membrane porosities as lithium-ion battery separators,” *Electrochim. Acta*, **236** 417–423 (2017). doi:10.1016/j.electacta.2017.03.205.
- 34) H. Fong, I. Chun, and D.H. Reneker, “Beaded nanofibers formed during electrospinning,” *Polymer (Guildf.)*, **40** (16) 4585–4592 (1999). doi:10.1016/S0032-3861(99)00068-3.
- 35) C. Huang, S. Chen, C. Lai, D.H. Reneker, H. Qiu, Y. Ye, and H. Hou, “Electrospun polymer nanofibres with small diameters,” *Nanotechnology*, **17** (6) 1558–1563 (2006). doi:10.1088/0957-4484/17/6/004.
- 36) J.E. Marshall, A. Zhenova, S. Roberts, T. Petchey, P. Zhu, C.E.J. Dancer, C.R. McElroy, E. Kendrick, and V. Goodship, “On the solubility and stability of polyvinylidene fluoride,” *Polymers (Basel)*, **13** (9) 1–31 (2021). doi:10.3390/polym13091354.
- 37) I.H. Peng, and C.H. Tu, “Densities and viscosities of acetone, diisopropyl ether, ethanol, and methyl ethyl ketone with a five-component hydrocarbon mixture from 288.15 k to 308.15 k,” *J. Chem. Eng. Data*, **47** (6) 1457–1461 (2002). doi:10.1021/je020077y.
- 38) D.B. Dwyer, E. E. Mera, G.S. Gudavalli, W.E. Bernier, T.P. Dhakal, and W.E. Jones, “Homogeneous titanium hydroxide yields hydroxyl decorated nanofiber separator with improved electrolyte uptake and device capacitance,” *Mater. Lett.*, **284** 129023 (2021). doi:10.1016/j.matlet.2020.129023.
- 39) B. Gao, S. Sinha, L. Fleming, and O. Zhou, “Alloy formation in nanostructured silicon,” *Adv. Mater.*, **13** (11) 816–819 (2001). doi:10.1002/1521-4095(200106)13:11<816::AID-ADMA816>3.0.CO;2-P.
- 40) S. Kaur, S. Sundarrajan, D. Rana, T. Matsuura, and S. Ramakrishna, “Influence of electrospun fiber size on the separation efficiency of thin film nanofiltration composite membrane,” *J. Memb. Sci.*, **392–393** 101–111 (2012). doi:10.1016/j.memsci.2011.12.005.
- 41) C.M. Costa, and S. Lanceros-Mendez, “Recent advances on battery separators based on poly(vinylidene fluoride) and its copolymers for lithium-ion battery applications,” *Curr. Opin. Electrochem.*, **29** 100752 (2021). doi:10.1016/j.coelec.2021.100752.
- 42) G. dong Kang, and Y. ming Cao, “Application and modification of poly(vinylidene fluoride) (pvdf) membranes - a review,” *J. Memb. Sci.*, **463** 145–165 (2014). doi:10.1016/j.memsci.2014.03.055.
- 43) K. Hwang, B. Kwon, and H. Byun, “Preparation of pvdf nanofiber membranes by electrospinning and their use as secondary battery separators,” *J. Memb. Sci.*, **378** (1–2) 111–116 (2011). doi:10.1016/j.memsci.2011.06.005.
- 44) "Acetone," n.d <https://webbook.nist.gov/cgi/cbook.cgi?ID=C67641&Mask=FFFF&Units=SI> (accessed October 10, 2021).
- 45) Ethanol," n.d <https://en.wikipedia.org/wiki/Ethanol> accessed October 10, 2021.
- 46) S. Czlonka, M.F. Bertino, J. Kośny, and N. Shukla, “Density and shrinkage as guiding criteria for the optimization of the thermal conductivity of poly(urethane)-class aerogels,” *J. Sol-Gel Sci. Technol.*, **93** (1) 149–167 (2020). doi:10.1007/s10971-019-05161-6.
- 47) C. Shao, H.Y. Kim, J. Gong, B. Ding, D.R. Lee, and S.J. Park, “Fiber mats of poly(vinyl alcohol)/silica composite via electrospinning,” *Mater. Lett.*, **57** (9–10) 1579–1584 (2003). doi:10.1016/S0167-577X(02)01036-4.
- 48) M. Li, L. Sheng, R. Xu, Y. Yang, Y. Bai, S. Song, G. Liu, T. Wang, X. Huang, and J. He, “Enhanced the mechanical strength of polyimide (pi) nanofiber separator via paali binder for lithium ion battery,” *Compos. Commun.*, **24** 100607 (2021). doi:10.1016/j.coco.2020.100607.